ACS Catalysis

Letter

pubs.acs.org/acscatalysis

Photocatalytic Fischer–Tropsch Synthesis on Graphene-Supported Worm-Like Ruthenium Nanostructures

Xiao-Ning Guo, Zhi-Feng Jiao, Guo-Qiang Jin, and Xiang-Yun Guo*

State Key Laboratory of Coal Conversion, Institute of Coal Chemistry, Chinese Academy of Sciences, Taiyuan 030001, China

Supporting Information

ABSTRACT: Fischer–Tropsch synthesis (FTS) converts carbon monoxide and hydrogen to liquid fuels and chemicals and is usually operated under high temperature ranges, which results in an evident increase of energy consumption and CO_2 emission. A photocatalytic FTS route was proposed to efficiently harvest solar energy. Worm-like ruthenium nanostructures dispersed on graphene sheets can effectively catalyze FTS at mild conditions (150 °C, 2.0 MPa H_2, and 1.0 MPa CO) under irradiation of visible light and achieve a catalytic activity as high as 14.4 $mol_{CO}{\cdot}mol_{Ru}{}^{-1}{\cdot}h^{-1}$. The reaction rate of FTS can be enhanced by increasing the irradiation intensity or decreasing the irradiation wavelength. The work provides a green and efficient photocatalytic route for FTS.

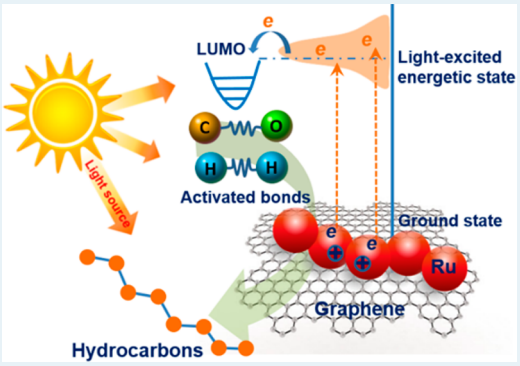

KEYWORDS: *photocatalysis, worm-like ruthenium nanostructures, Fischer–Tropsch synthesis, graphene, light-enhanced activity, production distribution*

Fischer–Tropsch synthesis (FTS), which converts carbon monoxide and hydrogen (syngas) to hydrocarbons, is an important process to produce liquid fuels and chemicals.[1−3] Traditional FTS employs coal-based syngas as the feedstock, and thus, it is hard to compete with the petroleum industry. With the increasing shortage of global fossil resources, the source of syngas has become diversified, including coal, natural gas, biomass, among others.[4−6] Meanwhile, the price of crude oil has also stayed at a high level. Therefore, FTS has gathered attention again for its ability to produce liquid fuels and chemicals from nonfossil resources. As syngas can be easily produced by biomass resource now, it would be a significant breakthrough if FTS could harvest sunlight—the most abundant energy source on the Earth.

Industrial FTS catalysts are usually based upon iron or cobalt conducting under high temperatures (310–340 °C for Fe catalysts or 210–260 °C for Co catalysts).[7] The high temperature leads to not only high energy consumption but also increased CO_2 emission due to the water–gas shift reaction.[8] Compared to Fe and Co, Ru catalysts are somewhat expensive, but they exhibit higher intrinsic activity, higher stability, and higher selectivity to long-chain hydrocarbons.[9,10] Besides, they are capable of operating in the presence of large amounts of water.[9,10] The presence of water, whether indigenous or co-fed, can lead to a significant increase in the reaction rate of FTS over Ru-based catalysts with decreasing CH_4 selectivity and increasing C_{5+} selectivity.[10] Ru is a nonplasmonic metal. Although it does not own the characteristic of so-called surface plasmon resonance,[11,12] its nanoparticles can also significantly absorb UV and visible light.[13,14] The light absorption of metal nanoparticles is generally attributed to the interband transition of bound electrons. Individual bound electrons gain the energy of incident photons and become "hot" electrons with high energy via the interband transition. These light-excited hot electrons in nanoparticles can facilitate chemical transformations of molecules adsorbed on the nanoparticles.[15−17] Recently, we found that graphene can stabilize some metastable nanoparticles, such as Cu_2O and Cu, and enable them to exhibit stable catalytic behavior.[17,18] Graphene is a two-dimensional network of sp^2-bonded carbon atoms,[19,] and the delocalized electrons in graphene can move freely in the network with a low resistance.[21] The carbon vacancies or dangling bonds in graphene can influence the electronic structure of metal atoms on graphene and improve their chemical stability.[22−24] Recent work by Moussa et al. shows that graphene as a support for FTS can exhibit a tunable metal–support interaction and lower water–gas shift activity.[25] Herein we report a novel visible light enhanced photocatalytic FTS (PFTS) process that employs graphene-supported worm-like Ru nanostructures as the catalyst.

The Ru/graphene catalyst was prepared by reducing ruthenium trichloride ($RuCl_3$) in the presence of poly(*N*-vinyl-2-pyrrolidone) (PVP) using 2.0 MPa H_2. The transmission electron microscope (TEM) images (Figure 1A, B and Figure S1) show that worm-like Ru nanostructures with a diameter of 2.2 nm and length of ∼10 nm are homogeneously dispersed on the graphene sheets. From the X-ray diffraction

Received: April 2, 2015
Revised: May 18, 2015
Published: May 19, 2015

DOI: 10.1021/acscatal.5b00697
ACS Catal. 2015, 5, 3836−3840

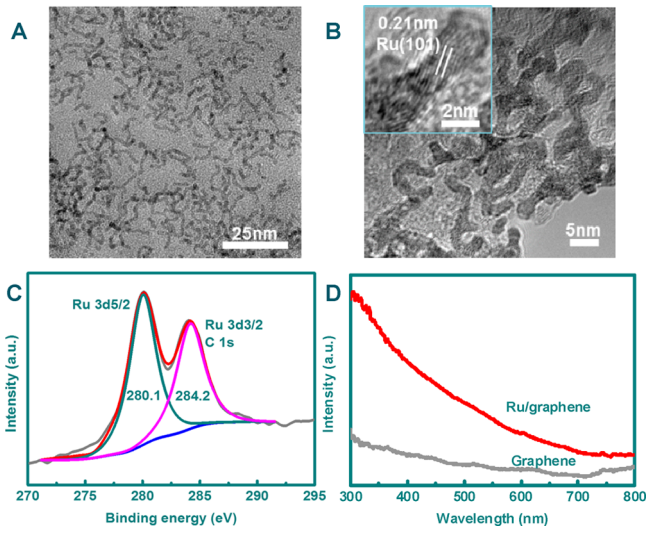

Figure 1. TEM images (A, B) and XPS profiles (C) of Ru/graphene and UV−vis absorption spectra of Ru/graphene and graphene (D). The inset in (B) is a HRTEM image of worm-like Ru nanostructures.

patterns (Figure S2), the diffractions corresponding to Ru(002) and Ru(101) can be observed at 42.1° and 44°. However, both diffraction peaks are so broad due to the small size of Ru crystals that they overlap with each other. From the XPS profiles (Figure 1C), the binding energies of Ru 3d5/2 and Ru 3d3/2 at 280.1 and 284.2 eV, respectively, can be attributed to the Ru^0 state. The above results confirm that Ru on the graphene sheets exists as the metallic phase. From the UV−vis spectra (Figure 1D), the Ru/graphene shows stronger light absorption than pure graphene, indicating that the enhanced light absorption originates from the worm-like Ru nanostructures dispersed on graphene sheets.

The PFTS process of Ru/graphene was carried out under mild conditions (2.0 MPa H_2, 1.0 MPa CO) and the irradiation of a 300 W Xe lamp, whose wavelength ranges from 400 to 800 nm. The reaction results are summarized in Table 1. The Ru/graphene exhibits high photocatalytic activity for FTS at 150 °C. The conversion of CO over the Ru/graphene is 43%, and the activity is 14.4 $mol_{CO}{\cdot}mol_{Ru}^{-1}{\cdot}h^{-1}$ (Table 1, entry 1). Without irradiation (dark reaction), the catalyst under the same temperature and pressure only shows an activity of 7.8 $mol_{CO}{\cdot}mol_{Ru}^{-1}{\cdot}h^{-1}$. This value is close to the result from Kou's group,[8] who developed an aqueous-phase process for FTS over Ru nanocluster catalyst. Therefore, the light-enhanced activity (the difference between the activity of light-irradiated reaction and reaction in the dark) is 6.6 $mol_{CO}{\cdot}mol_{Ru}^{-1}{\cdot}h^{-1}$.The above results indicate that the irradiation of visible light can significantly enhance the intrinsic catalytic ability of Ru/graphene for FTS. When CO molecules are adsorbed on Ru active sites, the electrons in the 5σ molecular orbitals of CO can transfer into the empty d orbitals of Ru to form Ru−C bonds.[26] Meanwhile, the back-donation of Ru d-orbital electrons into the empty 2π* orbitals of CO molecules can weaken the C−O strength and thus activate and dissociate CO molecules, a key step that largely determines the activity of FTS.[9,27] Bonn et al. found that laser pulse excitation of a ruthenium surface on which CO and atomic oxygen are coadsorbed gives rise to the formation of CO_2, whereas heating leads exclusively to desorption of carbon monoxide.[28,29] The CO oxidation reaction is mainly initiated by energetic hot electrons exciting by laser pulse, whereas the CO desorption is caused by coupling of the adsorbate to the phonon bath of the ruthenium substrate. Therefore, irradiation can effectively promote the activation of CO. In our case, the light irradiation usually excites bound electrons to a high-energy band through interband transitions. The excited electrons with sufficiently high energy are injected into the 2π* orbitals of CO molecules adsorbed on Ru sites, and this can significantly increase the rate of CO dissociation and then improve the catalytic activity.

The impact of the light intensity on the catalytic reaction rate was investigated by varying the irradiance while maintaining other experimental conditions unchanged at 150 °C.When the light intensity decreases from 0.5 to 0.4, 0.3, 0.2, and 0.1 W/cm^2, the catalytic activity linearly decreases from 14.4 to 13.2, 12.0, 10.5, and 9.4 $mol_{CO}{\cdot}mol_{Ru}^{-1}{\cdot}h^{-1}$, respectively (Table 1, entries 1−5, Figure S3A). The damping in the catalytic activity is due to the decrease in the number of energetic electrons at lower irradiation intensity. The product distributions under different light intensities have not evident difference (Figure S3B). However, all the C_{5+} hydrocarbon selectivities under irradiation are higher than that without irradiation, while the CH_4 and C_2−C_4 selectivities are lower (Figure S3B), suggesting that the irradiation can benefit the chain growth in PFTS. Hensen et al. found that the preferred chain growth of FTS over Ru base catalysts is the carbide mechanism (preferred path CH + CH coupling) because its overall barrier is lower than

Table 1. Performances of Ru/Graphene for PFTS under Different Reaction Conditions[a]

entry	catalyst	light intensity (W/cm^2)	temperature (°C)	activity ($mol_{CO}{\cdot}mol_{Ru}^{-1}{\cdot}h^{-1}$)
1	Ru/graphene	0.5	150	14.4(7.8)[b]
2	Ru/graphene	0.4	150	13.2
3	Ru/graphene	0.3	150	12.0
4	Ru/graphene	0.2	150	10.5
5	Ru/graphene	0.1	150	9.4
6	graphene	0.5	150	not detected
7	Ru/graphene	0.5	140	10.2(4.6)
8	Ru/graphene	0.5	130	7.1(3.0)
9	Ru/graphene	0.5	120	4.2(1.8)
10	Ru/graphene	0.5	110	2.9(0.9)
11	Ru/graphene	0.5	100	1.7(0.5)

[a]Catalytic tests were performed over 30 mg Ru/graphene (containing 0.2 mmol Ru) under 2.0 MPa H_2 and 1.0 MPa CO and the irradiation of a 300 W Xe lamp, whose wavelengths range from 400 to 800 nm. The catalytic activity is represented by moles of CO converted to hydrocarbons per mol of Ru per hour. [b]Values in parentheses show the catalytic activity without irradiation (dark reaction).

DOI: 10.1021/acscatal.5b00697
ACS Catal. 2015, 5, 3836−3840

that for chain growth in the CO insertion mechanism (preferred path C + CO coupling).[30,31] The main surface intermediate for chain propagating is CH via CH + CH and CH + CR (R = alkyl) coupling. In the transition state for CH + CH coupling, Pauli repulsion will be decreased by electron donation from two CH fragments to metal centers due to the overlap between bonding C−C orbitals and Ru d-band, which is in favor of the coupling. Under irradiation, the interband transition of Ru-bound electrons resulting form light exciation will increase the unsaturation of d-band.[16] This results in the donation of more electrons from two CH fragments to metal centers, which can further decrease the Pauli repulsion and then lower the energy barrier and increase the rate of the chain growth.

To test the role of graphene in the reaction, control experiments were conducted. No reaction product was detected in the blank experiment using only graphene as the photocatalyst (Table 1, entry 6). SiO_2 is a dielectric support, and it does not actively take part in the chemical reaction,[32] and therefore, Ru/SiO_2 (TEM images showing in Figure S4) with the same Ru loadings as Ru/graphene was also prepared and used as catalyst for FTS. The catalytic activities of 13.5 and 7.6 $mol_{CO}·mol_{Ru}^{-1}·h^{-1}$ were obtained with and without irradiation, respectively. The light-enhanced activity is 5.9 $mol_{CO}·mol_{Ru}^{-1}·h^{-1}$, which is smaller than that over Ru/graphene, indicating that graphene as support also can improve the reaction activity. Jarillo-Herrero et al. found that hot carrier-assisted intrinsic photoresponse in graphene can generate strong photocurrent.[33] The work function (WF) of graphene is about 4.5 eV, and the WF of Ru is 4.71 eV. Due to the different WFs, a built-in potential of 0.21 eV is formed near the junction between graphene and Ru. Because the WF of graphene is lower than Ru, the hot electrons with high energy can easily transfer to Ru from graphene. This can also result in a collection of energetic electrons at the Ru sites to further accelerate the reaction.

Generally, the reaction temperature greatly affects the catalytic activity. When the temperature decreases, the activity sharply reduces whether under irradiation or not (Table 1, entries 1 and 7−11). These results suggest that the reaction temperature also plays an important role in PFTS. Higher temperature can give rise to an increase in the quantity of adsorbed reactant molecules in excited states as dictated by the Bose−Einstein distribution,[34] which means that the reactant molecules require less energy to overcome the reaction barrier. Meanwhile, increasing the reaction temperature can also lead to a redistribution of electrons in Ru nanoparticles to higher energy levels.[34,35] The increased number of energetic electrons results in an enlarged probability that the energetic electrons activate the reactant molecules adsorbed on the Ru surface and to overcome the reaction barrier. The catalytic activity of Ru/graphene under irradiation is nearly two or three times as that without irradiation at experimental temperatures. Graphene has an excellent thermal conductivity.[36−38] Employing graphene as the support can effectively transfer the reaction heat of Ru surface. Moreover, the reaction temperature was strictly controlled by oil bath to ensure the temperature uniformity in the whole system. Therefore, the enhanced activity mainly results from the light irradiation rather than the local temperature increasing of catalyst. This suggests that the energy of electrons can be further raised by absorbing irradiation light, which further enhance the reaction activity. Therefore, the PFTS on the Ru/graphene is driven by effective coupling of thermal and light energy sources.

From Table 1, it is apparent that the activity of dark reaction at 120 °C (or 130 °C) is similar to that of light reaction at 100 °C (or 110 °C), but the product distributions under these reaction conditions are totally different (Figure 2, Table S1).

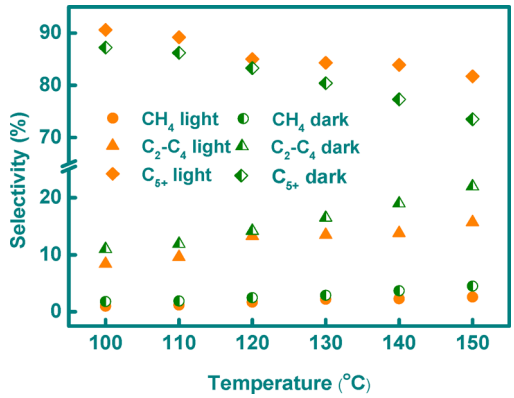

Figure 2. Selectivities of PFTS hydrocarbons with or without irradiation at different temperatures.

C_{5+} hydrocarbons have higher selectivities under irradiation, which further confirms the above. Whether under irradiation or not, the selectivity of C_{5+} hydrocarbons decreases with the increase of temperature, while the trend of CH_4 and C_2−C_4 selectivities are opposite. According to density functional theory study, the CH_4 formation has the highest barrier among the CH_x (x = 0−3) active species hydrogenation steps, and the barrier is also more than that of CH + CH or CH + CR (R = alkyl) coupling, indicating that CH_4 formation needs more energy.[31] In addition, CH + CR coupling is easier than coupling reactions of the type CH + CH because of the σ-donating effect of the alkyl substituent.[31] That is, the formation of light hydrocarbons also needs more energy to overcome the barrier. Therefore, the selectivity of light hydrocarbons is lower that of higher hydrocarbons at lower temperature. However, increased temperature can enhance the selectivity of light hydrocarbons.

The apparent activation energy of the FTS reaction under light irradiation and in the dark can be obtained by fitting the reaction data taken at different temperatures in the range of 100−150 °C to the Arrhenius eq (Figure S5). The apparent activation energy for the FTS in the dark is ∼72 kJ/mol, while it is ∼56 kJ/mol for the reaction under irradiation. The difference (ΔE_a = 16 kJ/mol) between them is the activation energy reduction by irradiation.

The distribution of PFTS products over Ru/graphene is shown in Table 2 and Figure S6. The selectivity of CO_2 over the catalyst is less than 1 mol %. This is mainly because the relatively low reaction temperature can effectively suppress the water−gas shift reaction.[2] Meanwhile, from the literature,[25] graphene as the catalyst support for FTS can also be conducive to reducing water−gas shift activity even at higher temperature. The hydrocarbons are the main products with a selectivity of 86.9 wt %, whereas the selectivity toward oxygenates (mainly alcohol) is 13.1 wt %. Among the hydrocarbons, C_{5+}hydrocarbons take the majority (81.7 wt %) of the products, and only 2.6 wt % of methane was formed. It is notable that the more useful olefins represent 56.4% of the whole C_2−C_4 hydrocarbons (gaseous products) (Figure 3A), suggesting that the Ru/graphene is a desirable catalyst for light olefins in the gaseous range. From Figure 3B, the selectivities of different hydrocarbon products follow the Anderson−Schulz−

DOI: 10.1021/acscatal.5b00697
ACS Catal. 2015, 5, 3836−3840

Table 2. Product Selectivity of Ru/Graphene in Different Wavelength Ranges[a]

wavelength range (nm)	400−800	500−800	600−800
total activity ($mol_{CO}·mol_{Ru}^{-1}·h^{-1}$)	14.4	11.3	8.9
light-enhanced activity ($mol_{CO}·mol_{Ru}^{-1}·h^{-1}$)	6.6	3.5	1.1
selectivities of products (wt %)			
hydrocarbons	86.9	85.4	85.0
oxygenates	13.1	14.6	15.0
distribution of hydrocarbon products (wt %)			
CH_4	2.6	3.1	3.9
C_2−C_4	15.7	16.3	17.1
C_5−C_{12}	59.1	57.0	58.2
C_{13}−C_{20}	19.1	19.7	17.6
C_{20+}	3.5	3.9	3.2

[a]Catalytic tests were performed over 30 mg Ru/graphene (containing 0.2 mmol Ru) under 2.0 MPa H_2 and 1.0 MPa CO at 150 °C and the irradiation of a 300 W Xe lamp, whose wavelengths range from 400 to 800 nm and light intensity is 0.5 W/cm^2. The product mixture consists of C_1 to C_{24} hydrocarbons. The selectivity of CO_2 over this catalyst is less than 1 mol %.

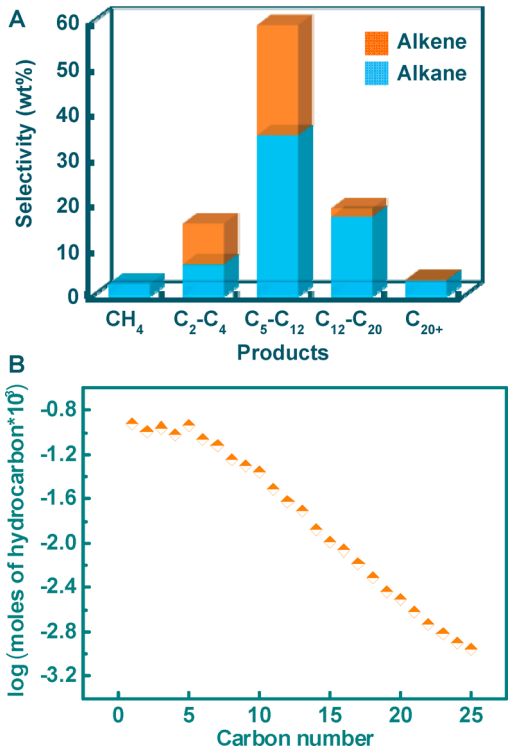

Figure 3. Selectivities of PFTS hydrocarbons (A) showing that the content of alkenes accounts for 56.4 wt % in C_2−C_4 hydrocarbons, and it rapidly decreases with the increase of carbon number. The Anderson−Schulz−Flory distribution of hydrocarbon products (B), suggesting a growth factor of 0.78.

Flory (ASF) distribution, with a growth factor (α) of hydrocarbon products of 0.78.

The dependence of the catalytic performance on the wavelength range of light was investigated. Without any filters, the light intensity and the reaction temperature was strictly controlled at 0.5 W/cm^2 and 150 °C, respectively. Then, a series of optical low-pass filters were employed to block light below specific cutoff wavelengths. The irradiation of the light with wavelengths ranging from 400 to 800 nm gives an activity of 14.4 $mol_{CO}·mol_{Ru}^{-1}·h^{-1}$. The activity decreases to 11.3 and 8.9 $mol_{CO}·mol_{Ru}^{-1}·h^{-1}$ when the wavelength range of the irradiation is 500−800 and 600−800 nm, respectively (Table 2). Because the activity in the dark is 7.8 $mol_{CO}·mol_{Ru}^{-1}·h^{-1}$, the light in the 600−800 nm wavelength range contributes 1.1 $mol_{CO}·mol_{Ru}^{-1}·h^{-1}$ (8.9−7.8), accounting for 7.6% (1.1/14.4 × 100%) of the total activity and 16.7% (1.1/(14.4−7.8) × 100%) of the light-induced activity. Similarly, the irradiation in the wavelength ranges of 400−500 and 500−600 contributes 3.1 (14.4−11.3) and 2.4 (11.3−8.9) $mol_{CO}·mol_{Ru}^{-1}·h^{-1}$, which acount for 46.9% and 36.4% of the light-induced activity, respectively. It can be seen that the highest activity in visible light range is observed in 400−500 nm, where the Ru nanochains strongly absorb the light (Figure S7A).

The impact of the specific irradiation wavelength on the catalytic activity was also studied. The method was the same as the study of dependence of activity on wavelength range, but the narrow band-pass filters were instead the low-pass filters. The light-enhaced activity decreases with the wavelength increase (Figure S7B). When the wavelength increases from (450 ± 10) to (500 ± 10), (550 ± 10), (600 ± 10), and (650 ± 10) nm, the light-enhaced activity decreases from 0.31 to 0.27, 0.21, 0.13, and 0.07 $mol_{CO}·mol_{Ru}^{-1}·h^{-1}$, respectively. This trend is similar to the absorption spectra of Ru/graphene. The photons with a shorter wavelength are able to excite metal electrons to higher energy levels, and these electrons are thus more effective in enhancing the reaction than those excited by photons with a longer wavelength. Therefore, the wavelength of light absorbed by the catalyst strongly influences the activity of PFTS reaction. For the Ru/graphene catalyst, however, the irradiation wavelength does not show significant impact on the distribution of PFTS products (Table 2). An experiment under the irradiation of ultraviolet light (<350 nm) was also conducted under the identical conditions. High activity of 16.5 $mol_{CO}·mol_{Ru}^{-1}·h^{-1}$(Table 2) is achieved. It is mainly because excited electrons with higher energy can accelerate the PFTS reaction.

To examine the stability of the Ru/graphene catalyst, the reaction was carried out in a semibatch mode for 30 h; that is, additional syngas was supplied to the reactor to restore the pressure to the initial value of 3.0 MPa every 5 h. The activity slightly dropped from 14.4 $mol_{CO}·mol_{Ru}^{-1}·h^{-1}$ at the beginning of the reaction to about 12.5 $mol_{CO}·mol_{Ru}^{-1}·h^{-1}$ after 10 h and then remained at this level over the next 20 h, thus demonstrating the long-term stability of the catalyst. The TEM image (Figure S8) of the catalyst used for 30 h showed no obvious change in morphology and aggregation of the worm-like Ru nanostructures. The X-ray diffraction results of the used catalyst did not show observable changes in the Ru

DOI: 10.1021/acscatal.5b00697
ACS Catal. 2015, 5, 3836−3840

phase either (Figure S2). When the used catalyst was treated in hydrogen atmosphere at 500 °C, its activity was restored to the level of the fresh Ru/graphene catalyst. This indicates that a slight oxidation of Ru nanostructures took place, most possibly at the surface of the Ru nanostructures during the photocatalytic process. The oxidation of Ru nanostructures led to the decline in their photocatalytic activity.

In summary, the present work demonstrates that Fischer–Tropsch synthesis, a very important artificial process for production of liquid fuels and chemicals, can be realized by an efficient photocatalytic route using Ru/graphene as the photocatalyst. The bound electrons in Ru nanostructures can absorb irradiation light via interband transitions and become energetic. These energetic electrons can transfer to reactant molecules and promote the chemical transformations between these molecules, and therefore, high temperature for promoting the reaction can be avoided. Moreover, the reaction rate of FTS can be enhanced by increasing the irradiation intensity or decreasing the irradiation wavelength. Because the non-plasmonic metals (such as Ru) have been widely used as the catalysts for various reactions, the reported discovery may significantly broaden the applications of catalytic processes driven by light.

■ ASSOCIATED CONTENT

Supporting Information

The Supporting Information is available free of charge on the ACS Publications website at DOI: 10.1021/acscatal.5b00697

Catalyst preparation and Characterizations, photocatalytic Fischer–Tropsch synthesis, and product detection, data anlysis, TEM, and XRD (PDF)

■ AUTHOR INFORMATION

Corresponding Author

*E-mail: xyguo@sxicc.ac.cn.

Notes

The authors declare no competing financial interest.

■ ACKNOWLEDGMENTS

The work was financially supported by National Basic Research Program (2011CB201405), NSFC (21403270 and 21473232), Shanxi Province (2013021007−1) and SKLCC (2014BWZ006).

■ REFERENCES

(1) Fischer, F.; Tropsch, H. *Ber. Dtsch. Chem. Ges. B* **1923**, *56*, 2428–2443.
(2) Khodakov, A. Y.; Chu, W.; Fongarland, P. *Chem. Rev.* **2007**, *107*, 1692–1744.
(3) de Klerk, A. *Energy Environ. Sci.* **2011**, *4*, 1177–1205.
(4) Huber, G. W.; Iborra, S.; Corma, A. *Chem. Rev.* **2006**, *106*, 4044–4098.
(5) Tran, N. H.; Kannangara, G. S. K. *Chem. Soc. Rev.* **2013**, *42*, 9454–9479.
(6) Luque, R.; de la Osa, A. R.; Campelo, J. M.; Romero, A. A.; Valverde, J. L.; Sanchez, P. *Energy Environ. Sci.* **2012**, *5*, 5186–5202.
(7) Leckel, D. *Energy Fuels* **2009**, *23*, 2342–2358.
(8) Xiao, C. X.; Cai, Z. P.; Wang, T.; Kou, Y.; Yan, N. *Angew. Chem., Int. Ed.* **2008**, *47*, 746–749.
(9) González-Carballo, J. M.; Pérez-Alonso, F. J.; Ojeda, M.; García-García, F. J.; Fierro, J. L. G.; Rojas, S. *ChemCatChem* **2014**, *6*, 2084–2094.
(10) Hibbitts, D. D.; Loveless, B. T.; Neurock, M.; Iglesia, E. *Angew. Chem., Int. Ed.* **2013**, *52*, 12273–12278.
(11) Marimuthu, A.; Zhang, J. W.; Linic, S. *Science* **2013**, *339*, 1590–1593.
(12) Ha, E.; Lee, L. Y. S.; Wang, J. C.; Li, F. H.; Wong, K. Y.; Tsang, S. C. E. *Adv. Mater.* **2014**, *26*, 3496–3500.
(13) Pakizeh, T. *J. Opt.* **2013**, *15*, 025001.
(14) Harpeness, R.; Peng, Z.; Liu, X.; Pol, V. G.; Koltypin, Y.; Gedanken, A. *J. Colloid Interface Sci.* **2005**, *287*, 678–684.
(15) Sarina, S.; Waclawik, E. R.; Zhu, H. Y. *Green Chem.* **2013**, *15*, 1814–1833.
(16) Sarina, S.; Zhu, H. Y.; Xiao, Q.; Jaatinen, E.; Jia, J. F.; Huang, Y. M.; Zheng, Z. F.; Wu, H. S. *Angew. Chem., Int. Ed.* **2014**, *53*, 2935–2940.
(17) Guo, X. N.; Hao, C. H.; Jin, G. Q.; Zhu, H. Y.; Guo, X. Y. *Angew. Chem., Int. Ed.* **2014**, *53*, 1973–1977.
(18) Yan, X. Y.; Tong, X. L.; Zhang, Y. F.; Han, X. D.; Wang, Y. Y.; Jin, G. Q.; Qin, Y.; Guo, X. Y. *Chem. Commun.* **2012**, *48*, 1892–1894.
(19) Novoselov, K. S.; Geim, A. K.; Morozov, S. V.; Jiang, D.; Zhang, Y.; Dubonos, S. V.; Grigorieva, I. V.; Firsov, A. A. *Science* **2004**, *306*, 666–669.
(20) Geim, A. K.; Novoselov, K. S. *Nat. Mater.* **2007**, *6*, 183–191.
(21) Geim, A. K. *Angew. Chem., Int. Ed.* **2011**, *50*, 6966–6985.
(22) Song, E. H.; Wen, Z.; Jiang, Q. *J. Phys. Chem. C* **2011**, *115*, 3678–3683.
(23) Mondal, P.; Sinha, A.; Salam, N.; Roy, A. S.; Jana, N. R.; Islam, S. M. *RSC Adv.* **2013**, *3*, 5615–5623.
(24) Yan, J. M.; Wang, Z. L.; Wang, H. L.; Jiang, Q. *J. Mater. Chem.* **2012**, *22*, 10990–10993.
(25) Moussa, S. O.; Panchakarla, L. S.; Ho, M. Q.; El-Shall, M. S. *ACS Catal.* **2014**, *4*, 535–545.
(26) Blyholder, G. *J. Phys. Chem.* **1964**, *68*, 2772–2778.
(27) Loveless, B. T.; Buda, C.; Neurock, M.; Iglesia, E. *J. Am. Chem. Soc.* **2013**, *135*, 6107–6121.
(28) Bonn, M.; Funk, S.; Hess, Ch.; Denzler, D. N.; Stampfl, C.; Scheffler, M.; Wolf, M.; Ertl, G. *Science* **1999**, *285*, 1042–1045.
(29) Hess, C.; Funk, S.; Bonn, M.; Denzler, D. N.; Wolf, M.; Ertl, G. *Appl. Phys. A: Mater. Sci. Process.* **2000**, *71*, 477–483.
(30) van Santen, R. A.; Markvoort, A. J.; Filot, I. A. W.; Ghouri, M. M.; Hensen, E. J. M. *Phys. Chem. Chem. Phys.* **2013**, *15*, 17038–17063.
(31) Filot, I. A. W.; van Santen, R. A.; Hensen, E. J. M. *Catal. Sci. Technol.* **2014**, *4*, 3129–3140.
(32) Mukherjee, S.; Zhou, L.; Goodman, A. M.; Large, N.; Ayala-Orozco, C.; Zhang, Y.; Nordlander, P.; Halas, N. J. *J. Am. Chem. Soc.* **2014**, *136*, 64–67.
(33) Gabor, N. M.; Song, J. C. W.; Ma, Q.; Nair, N. L.; Taychatanapat, T.; Watanabe, K.; Taniguchi, T.; Levitov, L. S.; Jarillo-Herrero, P. *Science* **2011**, *334*, 648–652.
(34) Christopher, P.; Xin, H. L.; Marimuthu, A.; Linic, S. *Nat. Mater.* **2012**, *11*, 1044–1050.
(35) Linic, S.; Christopher, P.; Ingram, D. B. *Nat. Mater.* **2011**, *10*, 911–921.
(36) Stankovich, S.; Dikin, D. A.; Dommett, G. H. B.; Kohlhaas, K. M.; Zimney, E. J.; Stach, E. A.; Piner, R. D.; Nguyen, S. T.; Ruoff, R. S. *Nature* **2006**, *442*, 282–286.
(37) Novoselov, K. S.; Fal'ko, V. I.; Colombo, L.; Gellert, P. R.; Schwab, M. G.; Kim, K. *Nature* **2012**, *490*, 192–200.
(38) Zhu, Y. W.; Murali, S.; Cai, W. W.; Li, X. S.; Suk, J. W.; Potts, J. R.; Ruoff, R. S. *Adv. Mater.* **2010**, *22*, 3906–3924.

■ NOTE ADDED AFTER ASAP PUBLICATION

This article was published ASAP on May 26, 2015 with an incorrect graph in Figure 1. The corrected version was reposted on May 27, 2015.

DOI: 10.1021/acscatal.5b00697
ACS Catal. 2015, 5, 3836–3840